Clays and Clay Minerals, Vol. 44, No. 4, 540–545, 1996.

REFINEMENT OF THE STRUCTURE OF NATURAL FERRIPHLOGOPITE

MARIA FRANCA BRIGATTI, LUCA MEDICI, AND LUCIANO POPPI

Dept. of Earth Sciences, University of Modena–Largo S. Eufemia, 19-41100 Modena, Italy

Abstract—Two ferriphlogopite-1*M* crystals with a composition $(K_{0.99}Na_{0.01})_{\Sigma=1.00}(Mg_{2.73}Fe^{2+}_{0.17}Fe^{3+}_{0.08}Ti_{0.01})_{\Sigma=2.99}[(Fe^{3+}_{0.95}Si_{3.05})_{\Sigma=4.00}O_{10.17}](OH)_{1.79}F_{0.04}$ (sample S1) and $(K_{1.02})_{\Sigma=1.02}(Mg_{2.68}Fe^{2+}_{0.20}Fe^{3+}_{0.11}Mn_{0.01})_{\Sigma=3.00}[(Fe^{3+}_{0.95}Si_{3.05})_{\Sigma=4.00}O_{10.18}](OH)_{1.75}F_{0.07}$ (sample S2) occur within an alkali-carbonatic complex near Tapira, Belo Horizonte, Minas Gerais, Brazil. Each crystal was studied by single-crystal X-ray diffraction. The least-squares refinements of space group *C2/m* resulted in R values of 0.031 for S1 and 0.025 for S2. Results showed that Fe^{3+} substitutes for Si within the tetrahedral sites and that the Fe distribution is fully disordered. The octahedral sites are preferentially occupied by Mg. The presence of Fe^{3+} within the tetrahedral sheet produces increased cell edge lengths. For sample S1, a = 5.362 Å, b = 9.288 Å, c = 10.321 Å and the monoclinic β angle was: β = 99.99°. For sample S2, a = 5.3649 Å, b = 9.2924 Å, c = 10.3255 Å and the monoclinic β angle was: β = 99.988°. The tetrahedral rotation angle of α = 11.5° is necessary for tetrahedral and octahedral sheet congruency. The enlarged tetrahedral sites are regular, with cations close to their geometric center. Ferriphlogopites have identical mean bond lengths for M1 and M2 sites within standard deviation. The M1-O3 and M2-O3 bond lengths are longer than the mean so that O3 may articulate with the tetrahedra.

Key Words—Crystal structure refinement, Ferriphlogopite.

INTRODUCTION

This paper reports the detailed crystal chemistry of a near end-member ferriphlogopite-1*M*. The crystals were obtained from an alkali-carbonatic complex outcropping near Tapira (Belo Horizonte, Minas Gerais, Brazil). Although evidence of Fe^{3+} tetrahedral substitution has been reported by several authors for trioctahedral true micas using chemical (Jakob 1925; Farmer and Boettcher 1981; Neal and Taylor 1989; Guidotti and Dyar 1991) and spectroscopic techniques (Dyar 1990; Rancourt et al. 1992, 1994), there are few structure refinements of crystals with Fe^{3+} substituting for Si^{4+} (Steinfink 1962; Donnay et al. 1964; Semenova et al. 1977, 1983; Hazen et al. 1981; Cruciani and Zanazzi 1994; Brigatti et al. 1995). Furthermore, there are no recent reports of natural trioctahedral micas without Al^{3+} and with octahedral and interlayer content close to end-member phlogopite.

Steinfink (1962) determined the crystal structure of a trioctahedral mica using precession and Weissenberg photographs. Its composition was: $(K_{0.9}Mn_{0.1})Mg_3Si_3(Fe,Mn)_1O_{10}(OH)_2$. From the structure refinement, Steinfink located Mn into the interlayer site and showed that iron produced tetrahedral ring distortion from hexagonal symmetry to one that involves tetrahedral rotations of approximately 12°. Donnay et al. (1964) derived ferriphlogopite structural parameters theoretically using unit-cell data and the crystal chemical composition reported by Steinfink (1962). The calculated values for some octahedral parameters disagree with those determined experimentally, because M1-O4 and M2-O3 distances are much greater than those found experimentally. Furthermore, Donnay et al. (1964), using the Weissenberg film technique, were the first to refine a synthetic ferriannite crystal. Complete refinement was not possible (final R = 9.3%) because of twinning. The ferriannite structure differed markedly from that of a crystal studied by Steinfink (1962). The ferriannite structure of Donnay had different coordinates for several atoms and it had a tetrahedral rotation angle of 6.3° whereas that of Steinfink was 12°.

Semenova et al. (1977), studied a ferriphlogopite of composition: $(K_{1.03}Na_{0.09}Ca_{0.04})_{\Sigma=1.16}(Mg_{2.89}Fe^{2+}_{0.16}Mn_{0.01})_{\Sigma=3.06}[(Al_{0.08}Fe^{3+}_{0.85}Ti^{4+}_{0.03}Si_{2.98})_{\Sigma=3.94}O_{10}](OH)_2$. Site occupancies are complex and are of non-integer values. They noted that, unlike other mica structures, tetrahedral Fe is located at the geometric center of the tetrahedron and that, as observed by Steinfink (1962), the tetrahedral rings deviate from hexagonal. The discovery of well-crystallized ferriphlogopite with a chemical composition close to that of end-member phlogopite provided an excellent opportunity to study the crystal chemistry of ferriphlogopite in detail. This

Table 1. Selected crystal data and unit cell parameters.

	S1	S2
a (Å)	5.362(1)	5.3649(4)
b (Å)	9.288(1)	9.2924(6)
c (Å)	10.321(2)	10.3255(9)
β (°)	99.99(1)	99.988(8)
V (Å^3)	506.2(1)	506.95(7)
N_{obs}	991	894
R_{sym} × 100	1.97	2.28
R_{obs} × 100	3.13	2.47

Note: $R_{sym} = (\Sigma_{hkl} \Sigma^N_{i=1}|I_{hkl} - I_{hkl}|)/(\Sigma_{hkl} \Sigma^N_{i=1} I_{hkl})$.

Table 2. Chemical data (a = weight %; b = unit cell content#) and mean atomic number (e^-) of octahedral (M) and interlayer (K) sites (c) for the refined ferriphlogopite crystals.

a			b			c	
	S1	S2		S1	S2	S1	S2
SiO_2	40.40	40.13	Si	3.05	3.05	M1 Xref	13.48(2)	13.78(5)
TiO_2	0.18	0.09	Fe^{3+}	0.95	0.95	M2 Xref	13.12(3)	13.53(3)
Fe_2O_3	18.06	18.55	[4]Sum	4.00	4.00	M1+M2 Xref†	39.7	40.8
FeO	2.74	3.15	Ti	0.01		M1+M2 EPMA‡	39.5	40.5
MgO	24.31	23.71	Fe^{3+}	0.08	0.11	K Xref	19.0(1)	19.46(4)
MnO	0.07	0.09	Fe^{2+}	0.17	0.20	K EPMA	18.8	19.4
BaO	0.09	0.04	Mg	2.73	2.68			
Na_2O	0.10	0.00	Mn		0.01			
K_2O	10.32	10.48	[6]Sum	2.99	3.00			
H_2O	3.55	3.45	Na	0.01				
F	0.18	0.31	K	0.99	1.02			
Sum	100.00	100.00	[12]Sum	1.00	1.02			
			OH	1.79	1.75			
			F	0.04	0.07			
			O	10.17	10.18			
			Sum	12.00	12.00			

Key: # calculated on the basis of $O_{12-x-y}(OH)_xF_y$. Xref = X-ray refinement; EPMA = electron microprobe; † (2M2+M1); ‡ = sum of octahedral cation electrons. Standard deviations are given in parentheses.

study and the refinement of the crystal symmetry is significant because previously refined crystal structures are of poor quality and involve crystals with complex chemical substitutions.

EXPERIMENTAL

Data Collection and Refinement

The two Al-free phlogopite crystals examined (sample Tas22-1: S1 and Tpq16-6B: S2) occur within ultramafics from near Tapira, 300 km West of Belo Horizonte, Minas Gerais, Brazil. Locality description, petrogenesis and data for host rock crystallization are given by Beurlen and Cassadanne (1981) and Brigatti et al. (1995). Crystals for the X-ray study were chosen from crushed rock. Only Al-free crystals whose precession photographs displayed sharp reflections and minimal spot streaking for $k \neq 3n$ reflections were selected. The absence of $h + k \neq 2n$ reflections confirmed the *C*-centered space group. The intensity distribution along rows (13*l*) and (02*l*) indicated the 1*M* polytype (Bailey 1988). Two crystals were selected; their dimensions were: sample S1 = 0.20 × 0.16 × 0.08 mm and sample S2 = 0.25 × 0.19 × 0.09 mm. Each crystal was mounted onto a Siemens P4 rotating-anode single-crystal diffractometer. The operating conditions were: Mo-Kα graphite-monochromatized radiation, operated at 40kV, 200mA and equipped with

Table 3. Final atomic fractional coordinates and equivalent isotropic (Å) and anisotropic (Å² × 10^4) thermal factors.

Atom	x/a	y/b	z/c	B_{eq}	β_{11}†	β_{22}†	β_{33}†	β_{12}†	β_{13}†	β_{23}†
	S1									
O1	−0.0024(5)	0.0	0.1705(2)	2.12(5)	212(8)	69(3)	36(2)	0	−1(3)	0
O2	0.3360(3)	0.2206(2)	0.1704(2)	2.14(4)	210(6)	78(2)	35(1)	−9(3)	25(2)	−10(1)
O3	0.1305(2)	0.1669(1)	0.3918(1)	0.61(2)	40(3)	14(1)	23(1)	−1(1)	10(1)	0(1)
O4	0.1335(3)	0.5	0.3990(2)	0.60(3)	41(4)	18(2)	19(1)	0	8(2)	0
T	0.07557(7)	0.16667(4)	0.22663(4)	0.64(1)	45(1)	17(1)	20(1)	0(1)	9(1)	0(1)
M1	0.0	0.0	0.5	0.54(2)	30(3)	12(1)	22(1)	0	9(1)	0
M2	0.0	0.33281(8)	0.5	0.48(1)	23(2)	11(1)	20(1)	0	9(1)	0
K	0.0	0.5	0.0	2.16(2)	206(3)	73(1)	40(1)	0	16(1)	0
	S2									
O1	−0.0020(4)	0.0	0.1705(2)	2.04(5)	194(8)	70(3)	33(2)	0	−11(3)	0
O2	0.3357(3)	0.2203(2)	0.1706(1)	2.02(4)	215(6)	69(2)	32(1)	−6(3)	19(2)	−10(1)
O3	0.1304(2)	0.1671(1)	0.3914(1)	0.62(2)	53(3)	14(1)	19(1)	2(1)	3(1)	0(1)
O4	0.1331(3)	0.5	0.3988(2)	0.61(3)	54(4)	16(2)	17(1)	0	6(2)	0
T	0.07552(7)	0.16664(4)	0.22666(3)	0.70(1)	62(1)	19(1)	19(1)	0(1)	6(1)	0(1)
M1	0.0	0.0	0.5	0.61(2)	48(3)	14(1)	20(1)	0	6(1)	0
M2	0.0	0.33280(8)	0.5	0.60(1)	47(2)	14(1)	20(1)	0	7(1)	0
K	0.0	0.5	0.0	2.11(2)	216(3)	72(1)	34(1)	0	10(1)	0

† $\exp[-(h^2\beta_{11} + \ldots + 2hk\beta_{12} + \ldots)]$. Standard deviations are given in parentheses.

https://doi.org/10.1346/CCMN.1996.0440413 Published online by Cambridge University Press

Table 4. Bond lengths (Å) and other important structural parameters.

	S1	S2		S1	S2
	Tetrahedron			Interlayer	
T-O1	1.680(1)	1.6804(9)	K-O1 (×2)	3.464(3)	3.464(2)
T-O2	1.679(2)	1.677(2)	K-O1′ (×2)	2.930(2)	2.933(2)
T-O2′	1.681(2)	1.684(2)	K-O2 (×4)	3.461(2)	3.464(2)
T-O3	1.678(1)	1.675(1)	K-O2′ (×4)	2.932(2)	2.934(2)
⟨T-O⟩	1.680	1.679	$\langle K\text{-}O\rangle_{inner}$	2.931	2.934
			$\langle K\text{-}O\rangle_{outer}$	3.462	3.464
			Δ⟨K-O⟩	0.531	0.530
	Octahedron M1			Octahedron M2	
M1-O3 (×4)	2.100(1)	2.105(1)	M2-O3 (×2)	2.094(1)	2.096(1)
M1-O4 (×2)	2.058(2)	2.062(2)	M2-O3′ (×2)	2.099(1)	2.102(1)
⟨M1-O⟩	2.086	2.091	M2-O4 (×2)	2.066(1)	2.068(1)
			⟨M2-O⟩	2.086	2.089
	Parameter				
Tetrahedral rotation α (°)				11.5	11.5
Basal oxygen Δz (Å)				0.001	0.001
Tetrahedral quadratic elongation TQE[1]				1.0000	1.0000
Tetrahedral angle variance TAV[1]				0.20	0.19
Tetrahedral bond length distorsion BLD_T[2] (%)				0.06	0.18
Tetrahedral angular distorsion AD_T[2] (%)				0.37	0.35
Tetrahedral edge length distorsion ELD_T[2] (%)				0.23	0.15
Tetrahedral basal edges mean bond length $\langle O\text{-}O\rangle_{basal}$ (Å)				2.736	2.738
Tetrahedral volume (Å^3)				2.431	2.429
Octahedral bond length distorsion BLD_M[2] (%)			M1	0.89	0.91
			M2	0.66	0.65
Octahedral volume (Å)			M1	11.907	11.983
			M2	11.904	11.950
Octahedral unshared edges mean bond length e_u[3] (Å)			M1	3.0967	3.1013
			M2	2.7967	2.8047
Octahedral shared edges mean bond length e_s[3] (Å)			M1	3.0967	3.0960
			M2	2.7967	2.8030
e_u/e_s[3]			M1	1.1073	1.1058
			M2	1.1073	1.1045
Sheet thickness (Å)					
Tetrahedral				2.277	2.272
Octahedral				2.151	2.159
Interlayer separation (Å)				3.459	3.466
Dimensional misfit Δ_{TM}[3] (Å)				0.629	0.618

Note: [1] Robinson et al. 1971; [2] Renner and Lehmann 1986; [3] Toraya 1981. Standard deviations are given in parentheses.

XSCANS software (Siemens 1993). Cell parameters were determined using least-squares refinement of 120 medium-high angle reflections. These values are given in Table 1 together with other information relative to data collection and refinement. The limiting spheres were sampled for the range $3 \leq 2\Theta \leq 70°$ ($-1 \leq h \leq 8$; $-14 \leq k \leq 14$; $-16 \leq l \leq 16$) using the ω scan window width of 2.6° for S1 and 1.5° for S2 and variable scanning speeds from 1 to 30°/min. Three standard reflections were checked every 100 reflections to monitor crystal and electronic stability. No instability was found. Lorentz-polarization corrections were made and absorption effects corrected using a complete ψ scan from 0–360° at 10° ψ intervals. There were ten selected reflections for S1 and fourteen for S2 ($\chi > 83°$). Intensity data of symmetrically-equivalent reflections were averaged and the resulting discrepancy factor (R_{sym}) calculated (Table 1).

The structure refinements were made by a full-matrix least-squares procedure. Reflections were selected with $I \geq 5\sigma$ (I) and using ORFLS (Busing et al. 1962). Atomic parameters from Brigatti and Davoli (1990) for space group *C2/m* were used as initial values for each refinement. Fully ionized scattering factors were used for octahedral M1 and M2 and ditrigonal K^+ sites. Mixed scattering factors (O/O^{2-}) were assumed for anion sites. A composite 75% Si and 25% Fe versus 75% Si^{4+} and 25% Fe^{3+} was used for tetrahedral sites. For the final steps of anisotropic refinement, scattering curves appropriate to composition were applied.

After refinement, the scattering contributions for H were examined for difference electron-density maps

https://doi.org/10.1346/CCMN.1996.0440413 Published online by Cambridge University Press

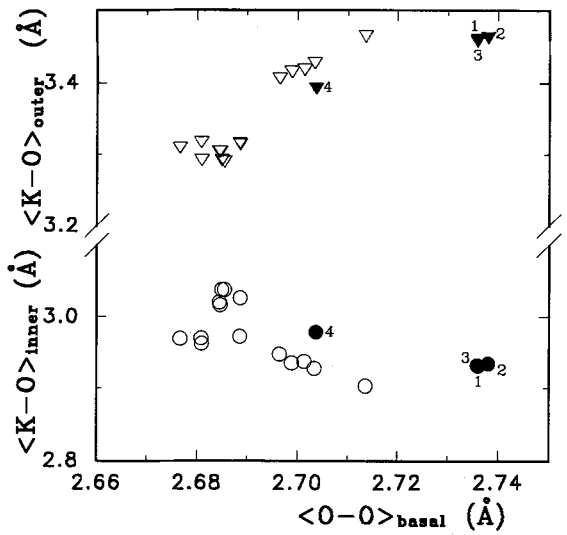

Figure 1. Variation of longer K-O mean bond length (triangles= $<K\text{-}O>_{outer}$) and shorter K-O mean bond length (circles= $<K\text{-}O>_{inner}$) vs. mean length of tetrahedral basal edges ($<O\text{-}O>_{basal}$). Filled symbols= $^{[4]}Fe^{3+}$-rich phlogopites, samples: 1 (S1) and 2 (S2) from this study, 3 from Semenova et al. (1977), and 4 from Brigatti et al. (1995). Open symbols= Al-rich phlogopites, phlogopites and biotites from literature (Alietti et al. 1995; Bigi and Brigatti 1994; Brigatti and Davoli 1990; Hazen and Burnham, 1973; Joswig 1972; Ohta et al. 1982; Takeda and Ross 1975).

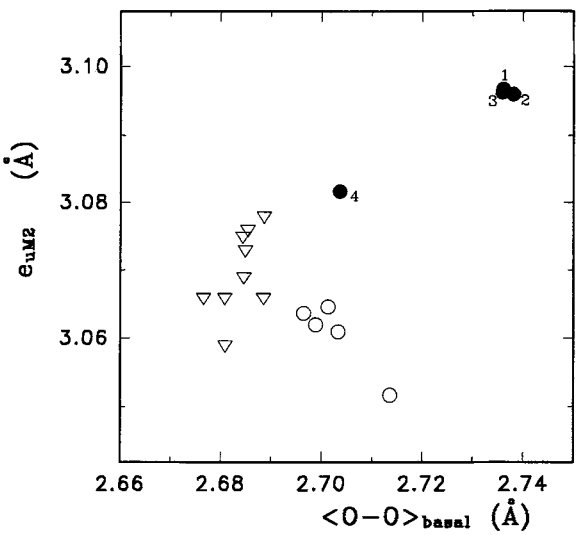

Figure 2. Length of unshared octahedral edges (e_{uM2}) vs. mean length of tetrahedral basal edges ($<O\text{-}O>_{basal}$). Symbols and samples as in Figure 1.

(DED). Small positive anomalies were found near the O4 atom (atomic coordinates = 0.11, 0.5, 0.33) suggesting that the OH vector is almost normal to plane (001). Nevertheless, O-H distances of 0.69 Å were shorter than expected one (0.95 Å) and their DED intensity was less than 4 σ above background. Thus, the H positions were not reliable and were not refined.

Average electron counts of cation sites are reported in Table 2. Atomic coordinates and temperature parameters are listed in Table 3. Relevant bond distances, selected tetrahedral, octahedral and interlayer parameters are reported in Table 4. Observed and calculated structure factors are available from the authors upon request.

Chemical Analyses

Electron-probe microanalysis (EPMA) were performed with an ARL-SEMQ instrument using wavelength-dispersive techniques. Operating conditions were 15-kV accelerating voltage, 15-nA sample current and a defocused electron beam (spot size of about 3 μm). The same crystals were used for both the refinement and the chemical analyses. Each analyzed crystal was chemically homogeneous. Semiquantitative scanning for all elements with $Z > 8$ did not reveal additional elements within detection limits. Ti and Ba contents were corrected for overlap of $Ti_{k\alpha}$ and $Ba_{L\alpha}$ peaks. The F^- was obtained following the method of Foley (1989). Chlorine was below the detection limit ($X < 0.001$ wt%). Crystals used for $(OH)^-$ and Fe^{2+} determination were obtained from the same samples that yielded the crystals used for the structure refinement. The weight loss was determined by thermogravimetric analysis in Ar gas to prevent Fe oxidation using a Seiko 5200 thermal analyzer. Heating rate was 10 °C/min and the flow rate was 200 ml/min. The Fe^{2+} was measured by the semi-microvolumetric method (Meyrowitz 1970). The oxide percentages and the structural formulae based on $O_{12-x-y}(OH)_xF_y$ are reported in Table 2.

DISCUSSION

The phlogopites studied lack Al and are deficient in Si, which accounts for Fe^{3+} tetrahedral substitution. Moreover, the phlogopites have a large quantity of Mg and a small quantity of Ti and Mn. Therefore, their octahedral composition is near to end-member phlogopite.

For phlogopites and biotites, the tetrahedral basal bond lengths increase as $^{[4]}Al$ substitutes for $^{[4]}Si$ and for Al-rich phlogopites, the increased substitution produces a more regular tetrahedra (Alietti et al. 1995). Fe^{3+}, a cation with a radius greater than Al^{3+}, emphasizes those effects (Table 4). Crystals with tetrahedral substitutions up to 24% are characterized by more regular (TQE = 1.0000; $ELD_T \leq 0.24$; $BLD_T \leq 0.0074$; $TAV \leq 0.20$; $AD_T \leq 0.37$; symbols as in Table 4) and larger tetrahedra ($<T\text{-}O> \geq 1.679$ Å) with increasing substitution. These features are also consonant with basal oxygen's low deviation from coplanarity ($\Delta z \leq 0.001$ Å). Moreover, the position of the tetrahedral cat-

https://doi.org/10.1346/CCMN.1996.0440413 Published online by Cambridge University Press

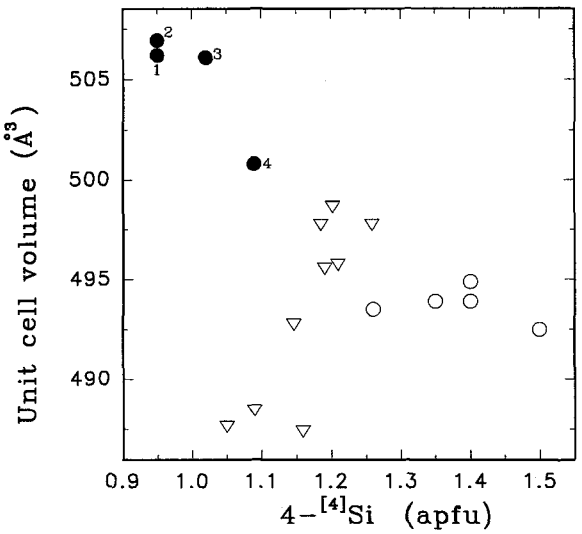

Figure 3. Unit-cell volume vs. the amount of tetrahedral substitution. Symbols and samples as in Figure 1.

ions, as indicated by individual T-O bond lengths and by BLD_T values, is near the middle of the polyhedron.

An increase of tetrahedral edge lengths (<O-O>basal) by Fe^{3+} substitution produces an increase of the tetrahedral sheet dimensions. This is also reflected within the geometry of the tetrahedral ring, with the reduction of the shorter K-O mean bond lengths ($<K-O>_{inner}$) (Figure 1). The increase of the longer K-O bond lengths ($<K-O>_{outer}$) can be produced not only by the presence in O4 position of $(OH)^-$ groups, as observed for muscovite (Guggenheim et al. 1987), but also occurs to match the lateral dimensions of the tetrahedral and octahedral sheets. The increase of ΔK ($<K-O>_{outer}$-$<K-O>_{inner}$) produces an increase in the distortion of the tetrahedral ring, which has angle values ($\alpha = 11.5°$) among the highest of those previously reported for trioctahedral 1*M* true micas.

M1 and M2 octahedral sites are approximately regular and their dimensions are similar, within experimental error. The M1 and, in particular, the M2 sites of the crystals studied are much larger and less distorted than those of other phlogopites.

The high values of the dimensional misfit (Δ_{TM}; $\Delta_{TM} > 0.61$ Å) between tetrahedral and octahedral sheets (Table 4) is mostly compensated for, as in all other micas, by an increased tetrahedral ring distortion. Other than an individual tetrahedron increase, there is a concomitant increase in the size of the octahedra. This is mostly reflected by the increased unshared edges of the M2 polyhedron (Figure 2).

As in phlogopite, the M-O3 distances are considerably larger than the M-O4 bond lengths for both M1 and M2 sites. Similar results are expected when monovalent F^- anions and/or (OH) groups occupy the O4 position (Guggenheim et al. 1987). The displacement of the central atom from the geometrical center of the polyhedron is toward O4 and the bond length distortion parameter BLD_M (Table 4) is slightly greater for the M1 site.

The large cell volumes relative to phlogopite are due to the lengthening of *a*, *b* and *c* cell parameters (Table 1). The β angles are among the lowest found for phlogopites-1*M*. Thus, we infer that the β angle is related to tetrahedral sheet composition. Figure 3 illustrates several relationships:

—for phlogopite-biotite crystals, the increase of Al is mostly related to exchange vectors balancing the octahedral charge increase. The most important exchange vector for Al-rich phlogopites is $^{[4]}Al^{3+}$-$^{[6]}Al^{3+}{}^{[4]}Si^{4+}_{-1}{}^{[6]}Mg^{2+}_{-1}$ and the unit-cell volume remains nearly constant. Whereas for biotite, the cell volume varies considerably, perhaps due to a complex set of exchange vectors affecting many cation sites.

—for ferriphlogopite crystals showing the main exchange vector $^{[4]}Fe^{3+}{}^{[4]}Al^{3+}_{-1}$, we observed a large increase of the unit-cell dimensions even for low tetrahedral substitution values. Cell volume, in accordance with other structural parameters, is mainly influenced by $^{[4]}Fe^{3+}$ content.

ACKNOWLEDGMENTS

The authors would like to acknowledge L. Beccaluva, F. Siena and C. Vaccaro for making rock specimens available for investigation, and E. Galli for their support and helpful discussions. The clarity of the manuscript was improved by critical readings by D. L. Bish, J. E. Mauk and an anonymous reviewer. This research was supported by MURST and CNR of Italy. The diffraction facilities were supported by Modena University (Centro Interdipartimentale Grandi Strumenti). The CNR is also acknowledged for financing the Electron Microprobe Laboratory at Modena University.

REFERENCES

Alietti E, Brigatti MF, Poppi L. 1995. The crystal structure and chemistry of high-aluminum phlogopites. Mineral Mag 59:149–157.

Bailey SW. 1988. X-ray diffraction identification of the polytypes of mica, serpentine, and chlorite. Clays & Clay Miner 36:195–213.

Beurlen H, Cassadanne JP. 1981. The brazilian mineral resources. Earth Sci Rev 17:177–206.

Bigi S, Brigatti MF. 1994. Crystal chemistry and microstructures of plutonic biotite. Am Mineral 79:63–72.

Brigatti MF, Davoli P. 1990. Crystal structure refinement of 1*M* plutonic biotites. Am Mineral 75:305–313.

Brigatti MF, Medici L, Saccani E, Vaccaro C. 1995. Phlogopites from the Alkaline-Carbonatite Complex of Tapira (Brazil): implications for their petrogenetical significance. Plinius 14:84–86.

Busing WR, Martin KO, Levi HS. 1962. ORFLS a FORTRAN crystallographic least-squares program. U.S. National Technical Information Service ORNL-TM-305.

Cruciani G, Zanazzi PF. 1994. Cation partitioning and substitution mechanisms in 1*M*-phlogopite: a crystal chemical study. Am Mineral 78:289–301.

Donnay G, Donnay JDH, Takeda H. 1964. Trioctahedral one-layer micas. II. Prediction of the structure from composition and cell dimensions. Acta Cryst 17:1374–1381.

Donnay G, Morimoto N, Takeda H, Donnay DH. 1964. Trioctahedral one-layer micas. I. Crystal structure of a synthetic iron mica. Acta Cryst 17:1369–1373.

Dyar MD. 1990. Mössbauer spectra of biotite from metapelites. Am Mineral 75:656–666.

Farmer GL, Boettcher AL. 1981. Petrologic and crystal chemical significance of some deep-seated phlogopites. Am Mineral 66:1154–1163.

Foley SF. 1989. Experimental constraints on phlogopite chemistry in lamproites: I. The effect of water activity and oxygen fugacity. Eur J Mineral 1:411–426.

Guggenheim S, Chang Y-H, Koster van Groos AF. 1987. Muscovite dehydroxylation: High-temperature studies. Am Mineral 72:537–550.

Guidotti CV, Dyar MD. 1991. Ferric iron in metamorphic biotites and its petrologic and crystallochemical implications. Am Mineral 76:161–175.

Hazen RM, Burnham CW. 1973. The crystal structures of one-layer phlogopite and annite. Am Mineral 58:889–900.

Hazen RM, Finger LW, Velde D. 1981. Crystal structure of a silica and alkali-rich trioctahedral mica. Am Mineral 66: 586–591.

Jakob J. 1925. X. beiträge zur chemischen konstitution der glimmer. I. Mitteilung die schwedischen manganophylle. Z Kristallogr 61:155–163.

Joswig W. 1972. Neutronenbeugungsmessungen an einem 1M-Phlogopit. N. Jahrbuch f. Mineralogie Monatshefte 1–11.

Meyrowitz R. 1970. New semimicroprocedure for determination of ferrous iron in refractory silicate minerals using a sodium metafluoborate decomposition. Anal Chem 42: 1110–1113.

Neal CR, Taylor LA. 1989. The petrography and composition of phlogopite micas from the Blue Ball kimberlite, Arkansas: a record of chemical evolution during crystallization. Mineral & Petrol 40:207–224.

Ohta T, Takeda H, Takéuchi Y. 1982. Mica polytypism: similarities in the crystal structures of coexisting 1*M* and 2*M*1 oxybiotite. Am Mineral 67:298–310.

Rancourt DG, Christie IAD, Royer M, Kodama H, Robert JL, Lalonde AE, Murad E. 1994. Determination of accurate $^{[4]}Fe^{3+}$, $^{[6]}Fe^{3+}$, and $^{[6]}Fe^{2+}$ site populations in synthetic annite by Mössbauer spectroscopy. Am Mineral 79:51–62.

Rancourt DG, Dang MZ, Lalonde AE. 1992. Mössbauer spectroscopy of tetrahedral Fe^{3+} in trioctahedral micas. Am Mineral 77:34–43.

Renner B, Lehmann G. 1986. Correlation of angular and bond length distortions in TO4 units in crystals. Z Kristallogr 175:43–59.

Robinson K, Gibbs GV, Ribbe PH. 1971. Quadratic elongation: a quantitative measure of distortion in coordination polyhedra. Science 172:567–570.

Semenova TF, Rozhdestvenskaya IV, Frank-Kamenetskii VA. 1977. Refinement of crystal structure of tetraferriphlogopite. Soviet Phys Crystall 22:680–683.

Semenova TF, Rozhdestvenskaya IV, Frank-Kamenetskii VA, Pavlishin VI. 1983. Crystal structure of tetraferriphlogopite and tetraferribiotite. Mineral Z 5:41–49 (in Russian).

Siemens 1993. XSCANS System—Technical reference Siemens Analytical X-ray Instruments.

Steinfink H. 1962. Crystal structure of a trioctahedral mica phlogopite. Am Mineral 47:886–896.

Takeda H, Ross M. 1975. Mica polytypism: dissimilarities in the crystal structures of coexisting 1*M* and 2*M*1 biotite. Am Mineral 60:1030–1040.

Toraya H. 1981. Distortions of octahedra and octahedral sheets in 1*M* micas and the relation to their stability. Z Kristallogr 157:173–190.

(Received 24 February 1995; accepted 13 November 1995; Ms. 2629)